RCS Advances

ARTICLE

# Design of thermoresponsive polymeric gates with opposite controlled release behaviors

Received 00th January 20xx,
Accepted 00th January 20xx

DOI: 10.1039/x0xx00000x

www.rsc.org/

Eduardo Guisasola[a,b], Alejandro Baeza[a,b], Marina Talelli[a], Daniel Arcos[a,b] and María Vallet-Regí[a,b]*

Stimuli-responsive devices are novel tools widely studied in the nanomedicine research field. In this work, magnetic-responsive mesoporous silica nanoparticles (MMSNs) were coated with an engineered thermoresponsive co-polymer. Magnetic cores are used as heating sources when they are exposed to an alternating magnetic field. The polymer structure suffers a change from hydrophilic to hydrophobic state when the temperature is raised above the lower critical solution temperature (LCST) or volume phase transition temperature (VPTT), acting as a gate-keeper of a model drug trapped inside the silica matrix. Fluorescein departure can be tuned employing two different polymer structures on the silica surface which exhibit the same transition temperature (42 ºC) but a different grafting density: one of them being a dense crosslinked polymer network and the other one a hairy linear polymer layer. The release profile reveals to be the opposite between these two different coatings, allowing suitable drug release behavior for different clinical situations.

## Introduction

Nanotechnology has risen as a powerful tool to improve the traditional techniques in chemical synthesis, therapies or devices, as well as developing new approaches for those research fields.[1,2] The combination of different chemical and physical properties at the nanoscale allows the development of sensors, drug delivery tools and nanomachines among others.[3–5] These devices have been extensively studied for their application in nanomedicine because they can transport cytotoxic drugs in their interior and be preferentially accumulated in solid tumors through the *enhanced permeation and retention effect* (EPR).[6] In order to apply the required therapy specifically in the tumor site, stimuli-responsive devices are good candidates due to the possibility of triggering the response only in the specific target zone. Different responsive moieties have been used to release the cargo by specific internal or external stimuli such as pH,[7] magnetic fields[8–10], redox processes[11], ultrasounds[12] and many others[13]. Among these different triggering stimuli, magnetic-responsive materials present interesting properties being able to produce different kinds of responses under DC or AC magnetic fields, i.e. the delivery of the devices to specific places,[14,15] or induce the magnetic nanoparticle heating.[16,17] Superparamagnetic iron oxide nanoparticles (SPION) are among the most studied nanocrystals for magnetic heating by an AC magnetic field exposure, therefore they have been used to induce physicochemical changes of specific moieties in the nanoparticle surroundings. For drug delivery purposes it is necessary to attach the cytotoxic agents on the surface of the magnetic nanoparticles[18] or design a matrix capable to retain those drugs.[19,20] Mesoporous silica nanoparticles (MMSN) have been widely used in this field by means of their stable mesoporous structure, easy surface functionalization, high surface area and other remarkable properties[21] that allow drug retention[22] and gate-keeper behavior.[23] Herein, SPIONs were embedded in the mesoporous silica matrix with intention to confer magnetic properties to the system. To build a stimuli-responsive device magnetic MMSNs were coated with a thermoresponsive polymer. This polymer decoration undergoes a hydrophilic to hydrophobic transition when is exposed to a temperature higher than its lower critical solution temperature (LCST).[24] The transition temperature of the well-known poly-N-isopropylacrylamide (pNIPAM) polymers is centered in 32 ºC, but it can be raised to higher temperatures by means of increasing the water-copolymer interactions introducing hydrophilic monomers such as N-hydroxymethyl acrylamide (NHMA).[25] Herein, we present a study about the role that the polymer grafting pathway plays in the release of fluorescein as a model drug. The polymer transition triggers or hampers the fluorophore departure according to the grafting procedure.

For crosslinked polymer shell coatings (CPS), the hydrophobic stacking of the polymer chains above the volume phase transition temperature (VPTT) leaves free spaces in the polymer network that allows the release of fluorescein

[a] Depto. Química Inorgánica y Bioinorgánica. Instituto de Investigación Sanitaria Hospital 12 de Octubre i+12 Universidad Complutense de Madrid. Plaza Ramon y Cajal s/n. E-mail: vallet@ucm.es
[b] Centro de Investigación Biomédica en Red de Bioingeniería, Biomateriales y Nanomedicina (CIBER-BBN), Av. Monforte de Lemos, 3-5. Pabellón 11. Planta 0 28029 Madrid, Spain

† Electronic Supplementary Information (ESI) available: See DOI: 10.1039/x0xx00000x

(Scheme 1a).[26] In the case of hairy polymer conformation (HP), the linear to globular transition that occurs in the surface of the mesoporous silica sterically hinders the pore opening causing the retention of the cargo (Scheme 1b).[27] Overall, it is demonstrated that coating with the same polymer but with a different grafting structure highly affects the fluorescein release behavior, rendering opposite profiles.

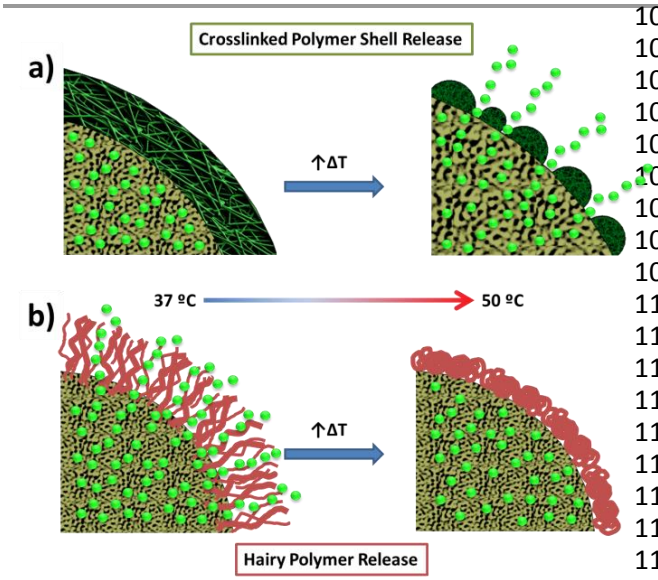


**Scheme 1.**Polymer behaviour for (a) crosslinked polymer shell coated magnetic mesoporous silica nanoparticles (MMSN@CPS) and (b) hairy polymer coated magnetic mesoporous silica nanoparticles (MMSN@HP).

## Experimental

### Materials

All chemicals were used without further purification. Tetraethyl orthosilicate (TEOS, 98 %), Cetyltrimethylammonium bromide (CTAB, 99%), aminopropyl triethoxysilane (APTES, 98%), [Tris(trimethoxy)silyl]propyl methacrylate (MPS, 98 %), Isopropylacrylamide (NIPAM, ≥99 %), (Hydroxymethyl)acrylamide solution (NHMA, 48 wt. % in $H_2O$), N,N'-Methylenebis(acrylamide) (MBA, 99 %) Oleic acid (OA, ≥99 %), 4,4'-Azobis(4-cyanovaleric acid) (ABCVA, ≥98.0%), aminopropyl triethoxysilane (APTES, 98%), fluorescein sodium salt, iron (II) chloride tetrahydrate ($FeCl_2{\cdot}4H_2O$, 99 %) and iron (III) chloride hexahydrate ($FeCl_3{\cdot}6H_2O$, >99%) were obtained from Sigma Aldrich. [Hydroxy(polyethyleneoxy)propyl] tri-ethoxysilane, (PEG-Si, MW = 575-750 g·mol$^{-1}$, 50 % in ethanol) was purchased from Gelest. Ammonium nitrate ($NH_4NO_3$, 99.9%), ammonium hydroxide ($NH_4OH$, 28-30 wt % as $NH_3$), chloroform ($CHCl_3$, 99.8 %), tetrahydrofuran (THF, 99.9 %), sodium hydroxide (NaOH, ≥98 %), absolute ethanol were purchased from Panreac. Ultrapure water was generated using a Millipore Milli-Q system with a Milli-pak filter of 0.22 µm pore size and used for all the preparation of aqueous solutions.

### Characterization Techniques.

Fourier transform infrared spectroscopy (FTIR) in a Thermo Nicolet nexus equipped with a Goldengate attenuated total reflectance device. The textural properties of the materials were determined by nitrogen sorption porosimetry by using a Micromeritics ASAP 2020. To perform the $N_2$ measurements, the samples were previously degassed under vacuum for 24 h at room temperature. Thermogravimetry analysis (TGA) were performed in a Perkin Elmer Pyris Diamond TG/DTA analyzer, with 5 °C min$^{-1}$ heating ramps, from room temperature to 600 °C. The hydrodynamic size of mesoporous and oleic acid iron oxide nanoparticles were measured by means of a Zetasizer Nano ZS (Malvern Instruments) equipped with a 633 nm "red" laser. Transmission electron microscopy (TEM) was carried out with a JEOL JEM 2100 instruments operated at 200 kV, equipped with a CCD camera (KeenView Camera). Sample preparation was performed by dispersing in distilled water and subsequent deposition onto carbon-coated copper grids. A solution of 1% of uranyl acetate (UA) was employed as staining agent in order to visualize the polymer coating attached on the mesoporous surface (Electron Microscopy Centre, UCM) using a graphite sample holder without any treatment. Liquid $^1$H-NMR experiments were made in a Bruker AV 250MHz. UV-Vis spectrometry was used to determine the LCST of linear polymers by means of a Biotek Synergy 4 device. DC magnetic field: magnetic parameters were determined by means of a vibrating sample magnetometer (VSM, Instituto de SistemasOptoelectrónicos y Microtecnología, Universidad Politécnica de Madrid, Spain).

### Calculation Procedures

The surface area was determined using the Brunauer-Emmett-Teller (BET) method and the pore volume (Vpore, cm$^3{\cdot}$g$^{-1}$), was estimated from the amount of $N_2$ adsorbed at a relative pressure around 0.99. The pore size distribution between 0.5 nm and 40 nm was calculated from the desorption branch of the isotherm by means of the Barrett-Joyner-Halenda (BJH) method. The mesopore size, Øpore (nm), was determined from the maximum of the pore size distribution curve. The mol percentage of NHMA ($f_{NHMA}$) in the synthesized block copolymers was determined using $^1$H NMR analysis using equation 1. $I_{4.66\ ppm}$ and $I_{3.87\ ppm}$ are the integrals of the protons at 4.66 ppm and 3.87 ppm respectively.

$$f_{NHMA}(\%) = \frac{I_{4.66\ ppm}/2}{I_{3.87\ ppm} + I_{4.66\ ppm}/2} \times 100 \qquad (1)$$

### Synthetic procedures

**Preparation of Hydrophobic Magnetite (OA-$Fe_3O_4$) NPs.** Hydrophobic magnetite NPs were synthesized by one-pot chemical coprecipitation method. Deionized water was purged with nitrogen gas for 10 min. Then, 4.80 g of $FeCl_3$•6H2O, 2.00 g $FeCl_2$•$4H_2O$, and 0.85 mL oleic acid were added to 30 mL of deionized water under nitrogen atmosphere with vigorous stirring. The mixture solution was heated to 90 ºC. Then, 20 mL of ammonium hydroxide (14 wt %) was added rapidly to the solution, and it immediately turned black. The reaction was kept at 90 ºC for 2.5 h and then allowed to cool to room

temperature. The black precipitate was collected by magnetic decantation and resuspended in chloroform with an end concentration of 32.8 mg·mL$^{-1}$ oleic acid-capped $Fe_3O_4$.

**Synthesis of ABCVA-APTES radical initiator.** To a 50 mL three-neck round-bottom flask, ABCVA (500 mg, 1.78 mmol) and NHS (460 mg, 3.915 mmol) were added and purged with nitrogen flow. Then, 25 mL of dry THF were added and the mixture was stirred at room temperature. Once the reactants were dissolved, DIC (1.22 mL, 7.87 mmol) was added dropwise and stirred for 1 h when a white precipitate is observed. Then, APTES (0.83 mL, 3.54 mmol) was added dropwise and the reaction mixture was stirred during 3 h prior to the reaction work-up. The white precipitate was removed by filtration (nylon, 0.2 µm) and the supernatant was evaporated under reduced pressure at 20 ºC. The dry product was dissolved in cold $CH_2Cl_2$ and a second white precipitate was observed and removed by filtration (nylon, 0.2 µm) prior to the separation by column chromatography over silica gel (heptane/EtOAc = 1:5). The product was subjected to a successive extraction with $Na_2HCO_3$ (5% wt), $NaHSO_4$ (5% wt) and brine, dried with $MgSO_4$ and the solvent evaporated under reduced pressure at 20 ºC to give an 85% purity product by $^1$H NMR.

$^1$H-NMR (250 MHz, $CDCl_3$), δ (ppm): 6.22 (s, 1H), 6.04 (s, 1H), 3.81 (q, J = 7.0 Hz, 12H), 3.33 – 3.14 (m, 4H), 2.52 – 2.08 (m, 8H), 1.74 (s, 3H), 1.69 (s, 3H), 1.66 – 1.59 (m, 4H), 1.22 (t, J = 7.0 Hz, 18H), 0.68 – 0.57 (m, 4H).

**Linear Thermoresponsive Polymer (TP-Si) Synthesis.** In a synthesis for a polymer with an 85:15 NIPAM to NHMA ratio, 1 g (8.8 mmol) of NIPAM and 355.6 µL (1.55 mmol) of NHMA were placed in vial A and 17.7 mg (0.024 mmol) of ABCVA-APTES initiator were placed in vial B. The monomer mixture and the initiator were purged by nitrogen flow prior to the addition of 6 mL and 0.5 mL of dry DMF respectively to each vial. The solutions were bubbled with $N_2$ for 15 min. Vial A was stirred in a heated oilbath at 80 ºC for 2 min before the fast addition of vial B solution (400:1 monomer to initiator ratio) and allowed to stir for 16 h. A maximum 2mL of the reaction mixture were added dropwise to 45 mL of $EtO_2$ in a centrifugation tube obtaining a white precipitate. The precipitate was washed three times with 45 mL of diethylether and dried at ambient temperature. The white solid was dissolved in $H_2O$ and lyophilized.

**Preparation of Mesoporous Magnetic Silica Nanoparticles (MMSNs).** MMSNs were prepared in a 50 mL round-bottom flask, adding 582 mg of CTAB as a phase transfer agent and structure-directing agent for silica condensation that were dissolved in 10 mL of $H_2O$ (mQ). Then, the mixture was mechanically stirred in an ultrasound bath during the addition of 26.4 mg OA-$Fe_3O_4$ in $CHCl_3$ (0.04 mL·min$^{-1}$ rate) until the complete removal of the organic solvent. The aqueous suspension was added through a 0.2 µm cellulose filter to an 86 mL NaOH (0.016M) solution and stirred at 600rpm. When the suspension was stabilized at 45 ºC, a mixture of 1.2 mL of EtOH and 1 mL of TEOS was added dropwise (0.25 mL·min$^{-1}$ rate). 15 min after TEOS addition was finished, 57.7 mg of sililated polymer (PEG-Si or TP-Si) were added, and the suspension was stirred for 2h. The reaction mixture was washed three times by centrifugation with 50 mL of $H_2O$, and then two more times with 50 mL of EtOH.

**MMSNs Crosslinked Polymer Shell Coating (MMSN@CPS).** The MMSNs coated with PEG chains were suspended in 200 mL of EtOH (99.5%). Then, 0.5 mL of MPS were added dropwise and the mix was kept stirring at 40 ºC during 16h. Before the washing step with absolute EtOH, the surfactant template was removed by ion exchange using 175mL of 10 g·L$^{-1}$ $NH_4NO_3$ in EtOH (95%) extracting solution at 65ºC overnight. The brown suspension was then centrifuged (15000 rpm, 30 min) and washed three times with 50 mL of EtOH to be dried under vacuum overnight. In a 100 mL three-neck round-bottom flask, 150.9 mg (1.33 mmol) of NIPAM, 12 mg of MBA (0.078mmol), 49.4 µL of NHMA (0.148 mmol), 3.6 mg of CTAB and 5 mg of $Na_2CO_3$ were added to 45 mL of $H_2O$ (mQ). The solution was stirred under $N_2$ bubbling at 70 ºC for 30 min to remove oxygen. Then, the solution was kept under $N_2$ and 50 mg of MMSNPs redispersed in 5 mL of EtOH (99.5%) were added to the monomer solution and stirred for 15 min more. To initiate the monomer polymerization 0.2 mL of a 25 mg·ml$^{-1}$ APS solution in $H_2O$ (mQ) previously deoxygenated were added to the reaction mixture. 20 min before the initiator addition appears a brown solid precipitate and the reaction mixture was allowed to cool down to room temperature and kept at that temperature for 6 h. The mixture was centrifuged and washed three times with $H_2O$ to remove the unreacted monomers and be dried under vacuum overnight.

**MMSNs Hairy Polymer Coating (MMSN@HP).** The MMSNs coated with TP-Si chains were dried under vacuum overnight. 50 mg of the brown solid were suspended in dry toluene to an end concentration of 1 mg·mL$^{-1}$ and 150 µL of MPS were added dropwise at room temperature. When the addition was ended, the temperature was raised to 100 ºC and kept under reflux during 16h. Before the washing step with absolute EtOH, the surfactant template was removed by ion exchange using 17.5mL of 10 g·L$^{-1}$ $NH_4NO_3$ in EtOH (95%) extracting solution at 65ºC overnight. The brown suspension was then centrifuged (15000 rpm, 30 min) and washed three times with 30 mL of EtOH to be dried under vacuum overnight. The brown solid so-obtained was purged by nitrogen flow and then dispersed in 5 mL of deoxygenated EtOH (99.5 %) with 269.2 mg of NIPAM and 116.5 µL of NHMA. Once the nanoparticles were well suspended and heated to 80 ºC, 100 µL of a second solution of ABCVA (17mg·mL$^{-1}$) in DMF was added and the mixture was stirred overnight. The product was washed with 30 mL of EtOH (99.5%) three times and dried over vacuum.

**Cargo Release Experiments.** Hybrid nanoparticles were loaded with a 20 mg·mL$^{-1}$ fluorescein sodium salt solution as a drug cargo model in PBS (1x) at 50 ºC for 32 h. Then, the hybrid material was washed with PBS (1x) until no fluorescence was observed. Fluorescein release experiments were carried out

with 5 mg of fluorescein loaded samples placed in a Corning® Transwell® inserts, dispersed in 0.2 mL and 0.8 mL of PBS in the bottom of the well. The samples were incubated at two different temperatures (37 ºC and 50 ºC) and fluorescence measurements were carried out taking 0.3 mL from the well and returned after every sample measurement.

## Results and Discussion

Tailoring heating responsive controlled release systems (CRSs) with opposite behavior relies on using the same copolymer NIPAM/NHMA as thermoresponsive gate, so that the model drug release is impelled or delayed above the VPTT or LCST respectively, depending on the polymerization strategy used in each case. Based on this hypothesis we envisioned the systems depicted in scheme 1 and developed two synthesis strategies represented in scheme 2. Both thermoresponsive CRSs are intended to work under the action of an AC magnetic field, so that the thermoseeds encapsulated within should increase the temperature on the MSNs surface above the polymer transition temperature.[28] In this work we have prepared oleic acid coated magnetite SPIONS thermoseeds.[29] The hydrophobic magnetic nanoparticles mean size was measured by transmission electron microscopy (TEM) and dynamic light scattering (DLS) in chloroform, showing a particle diameter of 7 nm (Figure S1). Our previous experiments[30] demonstrated that SPIONs as small as 7 nm can heat the MSNs surfaces up to 42 ºC under AC fields of 20.05 kA·m$^{-1}$ and 838 kHz. The hydrophobic magnetite nanoparticles were transferred to aqueous phase using a CTAB solution. Once this mixture is poured in the reaction media, CTAB micelles act as a template for the silica growth and SPIONS as silica nucleation spots after the TEOS addition, thus obtaining MMSNs.

Based on previous results about the heating power of our SPIONs mentioned above, diverse polymer transition temperatures were obtained by radical polymerization using different NIPAM/NHMA monomer feed ratios to find the desired polymer transition temperature range above physiological temperature (41 ºC to 43 ºC). Polymer transition temperatures were measured by UV-Vis spectroscopy finding that the 90:10 NIPAM/NHMA ratio (PL10, Figure S2), determined by $^1$H-NMR integration of NIPAM/NHMA signals, corresponds to a LCST at 42 ºC. To obtain an anchoring moiety in the thermoresponsive polymer chains, a sylilated initiator was synthesized by reacting 4,4'-Azobis(4-cyanovaleric acid) (ABCVA) with 3-aminopropyl triethoxysilane (APTES) and characterized by $^1$H-NMR and $^1$H-COSY (Figures S3 and S4). This monomer ratio was used for both polymer coatings, with the introduction of N,N-Methylenebis(acrylamide) (MBA) as cross-linking agent for the shell coating.

Prior to the polymer coating step, it is necessary to achieve a suitable colloidal stability in order to yield an efficient and homogeneous thermosensitive polymer layer on the particle surface. Several hydrophilic polymers can be used for this aim, e. g. polyethyleneglycol (PEG) through silica surface passivation[29] or PVP as an external stabilizing agent.[31] In this work, two different surface decorations were used to achieve the appropriate nanoparticle precursor prior to the polymerization step, dependent on the aimed small molecule release behavior. To obtain a higher cargo release at temperatures above the VPTT, the passivation process to confer colloidal stability was carried out with silylated PEG (PEG-Si), followed by the surface decoration with methacrylate moieties (MPS) that leads to the first precursor MMSN-PEG/MPS. For a reverse release profile, i.e. higher cargo release below LCST, functionalization of the silica surface was carried out with the addition of a preformed linear thermoresponsive silylated copolymer (TP-Si) added after the nanoparticle growth. Then, methacrylate moieties were attached to the silica surface to obtain the second precursor MMSN-TP/MPS (**Scheme 2**).

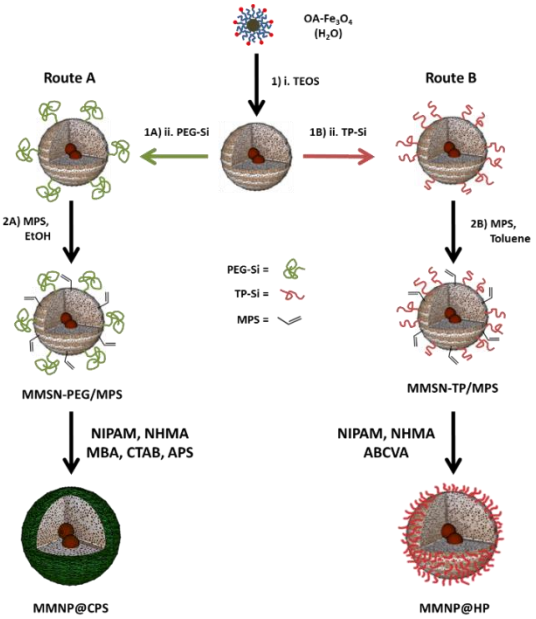


**Scheme 2**. Synthesis path for polymer shell coated MMSN@CPS (Route A) and hairy polymeric coated nanoparticles MMSN@HP (Route B).

Once obtained the respective stable nanoparticle systems, two different synthetic pathways were used in order to achieve the desired release profile. First one, a dense polymeric shell coating (MMSN@CPS) was obtained employing the MBA cross-linker addition (Route A, Scheme 2). The polymerization was performed on the silica surface of MMSN-PEG/MPS with NIPAM, NHMA and APS as initiator in aqueous media. The addition of the cationic surfactant CTAB in the polymerization step reveals critical to yield an effective polymeric coating. It is hypothesized that the electrostatic interactions between the negative charged silica surface and the cationic head of CTAB improves the approach of the non-charged monomers to the nanoparticle surface, as they would be in between the hydrophobic tail of CTAB. To prove this point, sodium dodecylsulfate (SDS) anionic surfactant was used in the polymerization step instead of CTAB and no polymeric coating was observed by thermogravimetric analysis or FTIR spectroscopy (data not shown). In the case of the hairy polymeric coating (MMSN@HP) the polymerization was

carried out in EtOH solution of the monomers NIPAM and NHMA with ABCVA as initiator (Route B, Scheme 2).

Finally, the devices were loaded with fluorescein sodium salt as a model drug. The release experiments were carried out in a Corning® Transwell® inset where 5 mg of material were dispersed in 1 mL of PBS. The samples were incubated at 37 ºC and 50 ºC respectively, monitoring the fluorescein release by fluorescence spectroscopy during 24 h. The release profile of MMSN@CPS shows a higher fluorescein amount of the sample placed at 50 ºC, while MMSN@HP sample at the same temperature shows only 20 % of fluorescein departure. The samples placed at 37 ºC work in the opposite manner, where MMSN@CPS undergo less fluorescein release than MMSN@HP, that loses its cargo because the polymer chains are not able to block the pore opening (Figure 1).

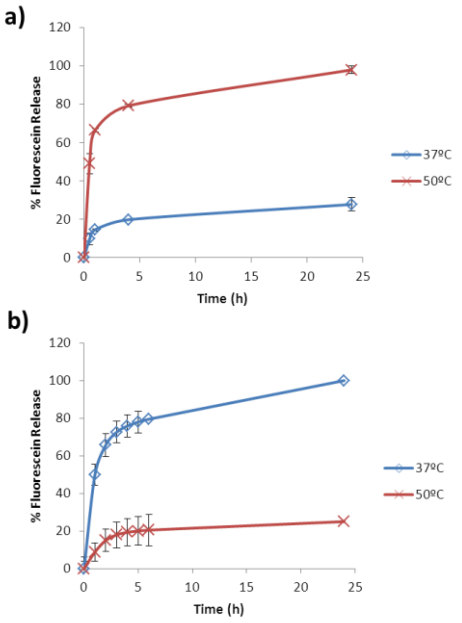


**Figure 1**. Release profiles for fluorescein loaded MMSN@CPS (a) and MMSN@HP (b).

Different characterization techniques have been used to have a deeper knowledge about the relation of the polymer structure and its behavior. The superparamagnetic behavior of the MMSNs provided by the iron oxide nanocrystals trapped in the silica matrix was confirmed by vibrating sample magnetometer (VSM), showing a magnetization curve with no hysteresis loop (figure 2). The maximum magnetization of the final polymer coated nanoparticles reaches values up to 10 % of the initial SPIONs (inset of figure 2). The fact that both systems present similar maximum magnetization values is in good agreement with the quantity of magnetite NPs incorporated within MMSNs, taking into account that the organic mass losses (34 %) by TGA are the same for the final devices MMSN@CPS and MMSN@HP (Figure S5), besides the silica matrix growth on the thermoseeds follows the same process to obtain both precursors.

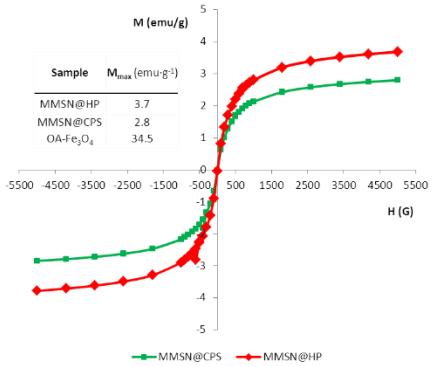


**Figure 2.** Vibrating Sample Magnetometer measurements of MMSNs with crosslinked polymer shell (MMSN@CPS) and hairy polymer (MMSN@HP) coatings.

Before MPS functionalization, the amount of polymer attached by *in situ* co-condensation in MMSNs was 5 % in both cases (data not shown). Then, TGA also reveals a functionalization with methacrylate moieties of 3 % for the MMSN-PEG/MPS which means a 25 % of final polymer attachment in MMSN@CPS (Figure S5a). The low amount of MPS groups show to be enough for polymer attachment, probably due to the assistance of the CTAB surfactant mentioned above. For MMSN-TP/MPS precursor, a 13 % of organic mass loss was assigned to the MPS functionalization and a 16 % assigned to the thermoresponsive final decoration (Figure S5b). In the case of MMSN@HP polymer grafting method, the amount of attached linear polymer determines the correct device operation. Therefore, if the density of linear polymer chains is low, the effective capping is compromised and thus does not prevent the fluorescein release when the polymer chains are shrunk. The presence of MPS for both precursors is confirmed by infrared spectroscopy (FTIR). In the case of MMSN-PEG/MPS, FTIR spectra shows a low intensity OC=O stretching band at 1700 $cm^{-1}$ that corresponds to methacrylate moiety, and the $C_{sp^3}$-H stretching band at 2900 $cm^{-1}$. Once the crosslinked polymer shell coating MMSN@CPS is obtained, the methacrylate band is not observable by FTIR, but two new bands become clearly visible at 1640 $cm^{-1}$, 1535 $cm^{-1}$ which can be assigned to secondary amide C=O stretching bonds (amide I and II bands). A broad band at 3300 $cm^{-1}$ correspond to N-H bending from the amide groups of the polymer coating and an increase of the $C_{sp^3}$-H asymmetric stretching band is attributed to the polymer backbone. The main bands at 1100 $cm^{-1}$ and 800 $cm^{-1}$ correspond to Si-O stretching and Si-O-Si bending respectively from the silica mesoporous matrix (figure 3a). The FTIR spectra of MMSN-TP/MPS is slightly different than the crosslinked polymer shell precursor due to the OC=O stretching band of MPS ester moiety is more intense, according with a higher amount of methacrylate groups obtained by TGA measurements. Besides, a second band at 1662 $cm^{-1}$ was found for this precursor which is in agreement with the presence of the NC=O stretching amide band from the thermoresponsive polymer chains attached during the MMSNs synthesis prior to the MPS functionalization.

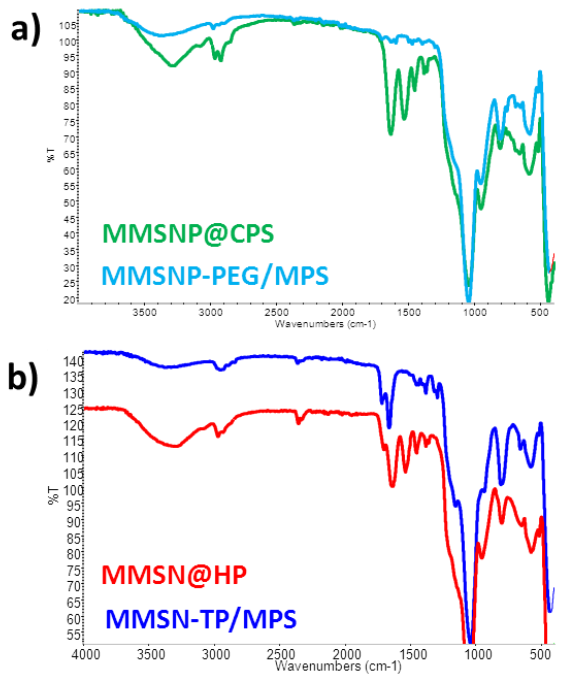


**Figure 3.** Fourier transform infrared spectroscopy of (a) MMSN@CPS and its precursor, and (b) MMSN@HP and its precursor.

The hairy polymer coating MMSN@HP obtained by linear radical polymerization has a similar FTIR spectra with MMSN@CPS which is expected because both coatings shares the same chemical nature. It is notable that the band corresponding to the methacrylate moiety has not completely disappeared after the polymerization step on the silica precursor surface (Figure 3b). This finding could mean that the linear polymer chains are formed mainly in the liquid phase and then, they are randomly attached on the particle through the methacrylate groups present on the surface. Therefore, many methacrylate groups remain unreacted due to steric hindrance of the grafted polymers. This fact is in agreement with the lower grafted polymer in comparison with MMSN@CPS according with TGA.

The zeta potential values measured for MMSN@HP and MMSN@CPS were −25.0 mV and −6.33 mV, respectively. Considering that the feed ratio of NIPAM/NHMA is the same in both samples the polymer structure should play a role in the difference in zeta potential. The dense cross-linked polymer network of MMSN@CPS could be responsible of blocking the negative charge of the silanol groups from the silica surface and provoking the higher zeta potential than the MMSN@HP sample, which are also in agreement with the previously discussed TGA an FTIR results. The lower zeta potential of MMSN@HP also suggests that the polymer layer on the surface is thin enough to expose the silanol groups along with the OH from the polymer structure. The BET surface area, pore volume and pore size measurements shows high values for both the uncapped precursors, but low values and pore size absence for the polymer capped ones (Figure S6). These findings reveal that the pore network blocking was achieved successfully by the polymer structures. Falta por hacer BET del Hairy polymer para confirmar.

The polymer coated magnetic mesoporous silica nanoparticles were obtained with 105 nm (figure 4a) of hydrodynamic diameter measured by dynamic light scattering (DLS) and confirmed by TEM images, which also reveal a good particle size, rounded shape (figure 4b-c, bottom image) and good porosity in the MMSNs precursors (figure 4b-c, upper image). The polymerization process slightly affects the particle aggregation in the case of MMSN@HP probably due to the high concentration of particles in the reaction media. The concentration in the linear polymeric coating step is crucial due to higher concentrations leads to gelification whereas lower concentrations do not yield an efficient nanoparticle coating (data not show). In the polymer shell coating process, lower nanoparticle aggregation is achieved thanks to the CTAB stabilization and higher dilution of the reaction medium (1mg·mL$^{-1}$). The TEM micrographs show that the PS coating is thicker than the HP decoration (Figure 4b-c, bottom) by staining the nanoparticle hybrids with 1% w/v solution of uranyl acetate (UA), as could be expected for a coating designed to be a dense polymer shell below the VPTT.

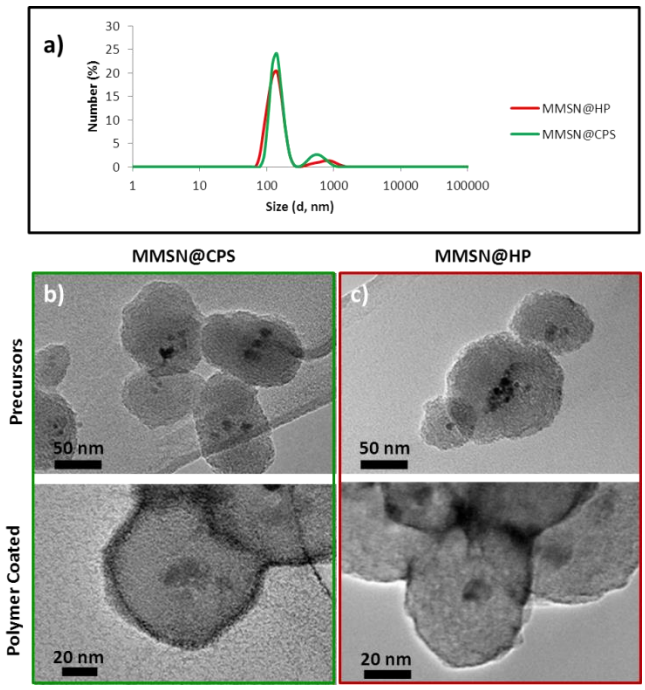


**Figure 4.** a) Hydrodinamic size for polymer coated nanoparticles. TEM micrographs of b) MMSN@CPS precursor (up) and MMSN@CPS (bottom). c) MMSN@HP precursor (up) and MMSN@HP (bottom).

The different grafting density and crosslinked nature of both systems determine the different fluorescein release behavior. On one hand when these polymers are in the hydrated state, the dense and highly crosslinked polymer shell present in MMSN@CPS act as a diffusion barrier which hampers the fluorophore departure, whereas the hairy polymer present in MMSN@HP cannot avoid the fluorescein leakage. In the latter system, when the polymer chain is in its hydrated state it does not present enough steric hindrance to produce an efficient pore closure but, if the temperature exceeds the LCST, its

globular state clogs the pore entrance avoiding the departure of the housed molecules. These polymer coatings ensure the colloidal stability of the device, which reveals critical for biomedical applications.[32]

In this work, we have developed two hybrid devices that demonstrate opposite release profiles taking advantage of the same hydrophilic to hydrophobic transition at 42 ºC. To this end, a tightly-packed crosslinked polymer shell was necessary to obtain a higher fluorescein release when heated above the VPTT. The heating power by an AC magnetic field through iron oxide thermoseeds of this kind of devices have been already tested and evidences the capacity of effectively addressing the local temperature required to trigger the cargo release. [30] An opposite release manner was obtained by the attachment of a linear thermosensitive copolymer on the silica nanoparticles surface. This reverse release behavior could be used in hyperthermia treatment taking advantage of the enhanced nanoparticle extravasation caused by the temperature increase[33] followed by the release of the drug trapped inside the pore walls only when the heating treatment is finished.

## Conclusions

In summary, a copolymer of NIPAM/NHMA monomers was grafted to the MMSNs by radical polymerization addressing two opposite release profiles. The different behavior comes from the polymer shell structure on the nanoparticles surface due to the chosen polymerization path. If the surface coating was carried with single strain thermoresponsive polymer, the polymer shrinkage blocks the pore entrance above the LCST hindering the fluorophore release, whereas a dense crosslinked polymer shell allows the model drug release due to the hydrophobic interactions between polymer chains creating aqueous channels in the polymer network above the VPTT. This methodology allows choosing the release profile for the required application.

## Acknowledgements

This work was supported by the Ministerio de Economía y Competitividad, through projects MAT2012-35556, MAT2013-43299R, and CSO2010-11384-E (Agening Network of Excellence). CIBER-BBN and ECO Foundation through project Smart4NB. CIBER-BBN is an initiative funded by the VI National R&D&i Plan 2008-2011, Iniciativa Ingenio 2010, Consolider Program, CIBER Actions, and financed by the Instituto de Salud Carlos III with assistance from the European Regional Development Fund. We also thank the NMR C.A.I., and the National Electron Microscopy Center, UCM. E.G. thanks CEI Campus Moncloa for the PICATA fellowship.

## References

1 R. K. Jain and T. Stylianopoulos, *Nat. Rev. Clin. Oncol.*, 2010, **7**, 653–664.

2 K. E. Sapsford, K. M. Tyner, B. J. Dair, J. R. Deschamps and L. Medintz, *Anal. Chem.*, 2011, **83**, 4453–4488.

3 K. Riehemann, S. W. Schneider, T. a. Luger, B. Godin, M. Ferrari and H. Fuchs, *Angew. Chemie - Int. Ed.*, 2009, **48**, 872–897.

4 A. Baeza, M. Colilla and M. Vallet-Regí, *Expert Opin. Drug Deliv.*, 2015, **12**, 319–337.

5 J. Wang and K. M. Manesh, *Small*, 2010, **6**, 338–345.

6 H. Maeda, H. Nakamura and J. Fang, *Adv. Drug Deliv. Rev.*, 2013, **65**, 71–79.

7 E. S. Lee, Z. Gao and Y. H. Bae, *J. Control. Release*, 2008, **132**, 164–170.

8 J. Thévenot, H. Oliveira, O. Sandre and S. Lecommandoux, *Chem. Soc. Rev.*, 2013, **42**, 7099–116.

9 J. E. Lee, N. Lee, T. Kim, J. Kim and T. Hyeon, *Acc. Chem. Res.*, 2011, **44**, 893–902.

10 C. R. Thomas, D. P. Ferris, J.-H. Lee, E. Choi, M. H. Cho, E. S. Kim, J. F. Stoddart, J. Shin, J. Cheon and J. I. Zink, *J. Am. Chem. Soc.*, 2010, **132**, 10623–5.

11 R. Liu, X. Zhao, T. Wu and P. Feng, *J. Am. Chem. Soc.*, 2008, **130**, 14418–14419.

12 J. L. Paris, M. V. Cabañas, M. Manzano and M. Vallet-Regí, *ACS Nano*, 2015, **9**, 11023–11033.

13 S. Mura, J. Nicolas and P. Couvreur, *Nat Mater*, 2013, **12**, 991–1003.

14 J. Cheng, B. a. Teply, S. Y. Jeong, C. H. Yim, D. Ho, I. Sherifi, S. Jon, O. C. Farokhzad, A. Khademhosseini and R. S. Langer, *Pharm. Res.*, 2006, **23**, 557–564.

15 M. Muthana, A. J. Kennerley, R. Hughes, J. Richardson, M. Paul, C. Murdoch, F. Wright, M. Lythgoe, N. Farrow, J. Dobson, J. M. Wild and C. Lewis, *Nat. Commun.*, 2013, **6**, 1–11.

16 S. Dutz and R. Hergt, *Int. J. Hyperthermia*, 2013, **29**, 790–800.

17 D. Yoo, H. Jeong, S.-H. Noh, J.-H. Lee and J. Cheon, *Angew. Chemie Int. Ed.*, 2013, **52**, 13047–13051.

18 A. Riedinger, P. Guardia, A. Curcio, M. A. Garcia, R. Cingolani, L. Manna and T. Pellegrino, *Nano Lett.*, 2013, **13**, 2399–2406.

19 N. S. Satarkar and J. Z. Hilt, *J. Control. Release*, 2008, **130**, 246–251.

20 X. Zhang, P. Yang, Y. Dai, P. Ma, X. Li, Z. Cheng, Z. Hou, X. Kang, C. Li and J. Lin, *Adv. Funct. Mater.*, 2013, **23**, 4067–4078.

21 F. Hoffmann, M. Cornelius, J. Morell and M. Fröba, *Angew. Chemie Int. Ed.*, 2006, **45**, 3216–3251.

22 M. Vallet-Regi, a. Rámila, R. P. Del Real and J. Pérez-Pariente, *Chem. Mater.*, 2001, **13**, 308–311.

23 S. Giret, M. Wong Chi Man and C. Carcel, *Chem. - A Eur. J.*, 2015, **21**, 13850–13865.

24 H. G. Schild, *Prog. Polym. Sci.*, 1992, **17**, 163–249.

25 R. Liu, M. Fraylich and B. R. Saunders, *Colloid Polym. Sci.*, 2009, **287**, 627–643.

26 J.-H. Park, Y.-H. Lee and S.-G. Oh, *Macromol. Chem. Phys.*, 2007, **208**, 2419–2427.

27 Y.-Z. You, K. K. Kalebaila, S. L. Brock and D. Oupický, *Chem. Mater.*, 2008, **20**, 3354–3359.

28 J. Dong and J. I. Zink, *ACS Nano*, 2014, **8**, 5199–5207.

29 Y.-S. S. Lin and C. L. Haynes, *Chem. Mater.*, 2009, **21**, 3979–3986.

30 E. Guisasola, A. Baeza, M. Talelli, D. Arcos, M. Moros, J. M. De La Fuente and M. Vallet-Regí, *Langmuir*, 2015, 2–7.

31 J. Cha, P. Cui and J.-K. Lee, *J. Mater. Chem.*, 2010, **20**, 5533.

32 Y.-S. Lin, K. R. Hurley and C. L. Haynes, *J. Phys. Chem. Lett.*, 2012, **3**, 364–374.

33 G. Kong, R. D. Braun and M. W. Dewhirst, *Cancer Res.*, 2001, **61**, 3027–3032.